Electronic and Nonlinear Optical Properties of 2-Methyl-4-Nitroaniline Clusters

CHAPTER · DECEMBER 2003

DOI: 10.1142/9789812564368_0002

READS

11

4 AUTHORS:

Maxime Guillaume

Solvay

35 PUBLICATIONS **729** CITATIONS

SEE PROFILE

Benoît Champagne

University of Namur

401 PUBLICATIONS **8,719** CITATIONS

SEE PROFILE

Frédéric Castet

Université of Bordeaux

90 PUBLICATIONS **1,691** CITATIONS

SEE PROFILE

Laurent Ducasse

Université Bordeaux 1

157 PUBLICATIONS **2,594** CITATIONS

SEE PROFILE

Electronic Excitations and First Hyperpolarizability of 2-Methyl-4-Nitroaniline Clusters

MAXIME GUILLAUME,[1] EDITH BOTEK,[1] BENOÎT CHAMPAGNE,[1] FRÉDÉRIC CASTET,[2] LAURENT DUCASSE[2]

[1]*Laboratoire de Chimie Théorique Appliquée, Facultés Universitaires Notre-Dame de la Paix, 61 rue de Bruxelles, B-5000 Namur, Belgium*

[2]*Laboratoire de Physico-Chimie Moléculaire, UMR 5803 CNRS, Université Bordeaux I, 33405 Talence, Cedex, France*

Received 23 February 2002; accepted 12 June 2002

DOI 10.1002/qua.10355

ABSTRACT: The crystal packing effects upon the static and dynamic first hyperpolarizability of 2-methyl-4-nitroaniline (MNA) clusters have been addressed at the TDHF/AM1 level. Due to electrostatic interactions, in 1-D arrays of MNA unit cells extending along the *a* crystallographic axis, the effective hyperpolarizability strongly increases whereas stacking unit cells along the *b* or *c* axes leads to a reduction of these quantities. These effects are magnified in the case of frequency-dependent quantities. The first hyperpolarizability variations can mostly be related to bathochromatic and hypsochromatic shifts as well as to changes in transition dipole moments of the low-energy excited states that dominate the UV/visible absorption spectra. From calculations performed at the CIS/INDO/S level of approximation, these dominant excited states present an important intramolecular charge transfer character and bathochromatic (hypsochromatic) shifts are associated with increase (decrease) of the transition dipole moments. In addition, a large number of intermolecular charge-transfer excited states have been detected. In the small MNA aggregates as well as in clusters extending only along the *b* or *c* crystallographic axes, these excited states possess small transition dipole moments. On the other hand, when stacking MNA unit cells along the *a* axis the electrostatic interactions induce a decrease of the excitation energies and an increase of the transition dipole moments of these intermolecular charge transfer states. As a consequence, they account for a nonnegligible contribution to the first hyperpolarizability. Int J Quantum Chem 90: 1378–1387, 2002

Key words: first hyperpolarizability; electronic excitation energies; charge transfer; molecular crystal; 2-methyl-4-nitroaniline

Correspondence to: B. Champagne; e-mail: benoit.champagne@fundp.ac.be

1. Introduction

Molecules presenting large second-order nonlinear optical (NLO) responses are good candidates to build advanced-technology devices such as electrooptical modulators and frequency mixers [1]. In addition to large responses at the microscopic level (β, the first hyperpolarizability), the material should exhibit large macroscopic responses ($\chi^{(2)}$, the second-order nonlinear susceptibility). The first requirement is in general achieved by conjugated molecules substituted at their extremities by donor/acceptor (D/A) groups. Numerous experimental [2] and theoretical [3, 4] investigations have been devoted to the maximization of β with respect to the nature and length of the conjugated segment as well as with respect to the nature, strength, and number of substituents. The second condition has received a lot of experimental attention in what concerns the "asymmetry requirement." Indeed, dipolar molecules tend to aggregate in a centrosymmetrical (or nearly centrosymmetrical) mode that ensures an optimal electrostatic stabilization to the detriment of the magnitude of $\chi^{(2)}$. Chromophores with small dipole moment, hydrogen bond networks, substituents (including these with chiral moieties), electric field poling, and cocrystallization are typical strategies that have been followed to enforce noncentrosymmetrical crystal packing. For instance, *p*-nitroaniline (*p*NA) crystallizes into a centrosymmetrical structure whereas 2-methyl-4-nitroaniline (MNA)—the compound that is obtained from *p*NA by substituting a methyl group for a ring hydrogen—crystals are noncentrosymmetrical [5].

As reviewed recently [6], contrary to investigations of isolated molecules, fewer studies have tackled the evaluation of the bulk nonlinear susceptibilities of molecular crystals and their relationships to crystal structure and intermolecular interactions. In addition to the oriented gas approximation, originally introduced by Chemla et al. [7] and that relies on the additivity of molecular hyperpolarizabilities, several interaction schemes have been elaborated to account for the shape, anisotropy, and spatial organization of molecules in the crystals. Dykstra [8] proposed a general "classic" approach where the intermolecular electrical interactions are accounted for through interacting (hyper)polarizable point-multipoles. Successive differentiations of the field-dependent interaction energy provide the various static linear and nonlinear responses of the clusters as illustrated by a recent study on *all-trans* hexatriene bundles [9]. In addition to the electrical phenomena, Munn incorporated electric field gradient and magnetic field effects [10] into the self-consistent procedure of determination of the local fields [11]. Many applications of Refs. [10, 11] to the calculation of the macroscopic NLO responses of molecular crystals have been carried out and addressed (1) the performance of various schemes of distributed (hyper)polarizabilities, (2) the magnitude of the permanent field effects, and (3) the choice of molecular wave functions [12, 13]. According to Zyss and Berthier [14], these developments already improve substantially over the oriented gas approximation because they include (or can include) multipolar potentials and dispersion contributions [8]. The model of Reis et al. [13] also includes the charge flow between different regions of the molecule, of particular relevance in many push–pull π-conjugated systems [3]. Nevertheless, (field-induced) intermolecular charge transfer effects upon the macroscopic NLO properties still deserve to be addressed in conjunction with classic approaches.

A straightforward alternative to the classic mutual polarization schemes is the supermolecule approach, where the crystal is modeled by representative molecular clusters. This technique enables taking into account the specific and nonadditive effects due to the intermolecular interactions but often suffers from their huge computational cost, which implies the use of semiempirical schemes. The supermolecule approach was used to elucidate the relationships between β and the relative orientation of *p*NA molecules in small clusters [15]. Hamada [16] has shown that for MNA dimers the supermolecule approach and the classic electrostatic treatment provide a similar picture of the intermolecular interaction effects upon β. By building increasingly large 1-D and 2-D clusters and using an AM1 Hamiltonian, two of us recently characterized the crystal packing effects upon the static first hyperpolarizability along each crystallographic axis of the MNA crystal [17]. On the one hand, it was shown that a simple multiplicative scheme can infer the first hyperpolarizability of 2-D clusters from the knowledge of the first hyperpolarizability of the corresponding 1-D arrays. On the other hand, the coupled Hartree–Fock approach (within its finite field (FF) version [18]) combined with AM1 Hamiltonian turned out to reproduce, for MNA dimers, the MP2 results of the packing effects upon β. Provided the clusters are large enough, the supermolecule approach, which can take into account all packing effects, provides the

bulk nonlinear susceptibility. Here, the difficulty arises from the extrapolation of the results obtained for clusters of finite size to the infinite crystal size. Indeed, Refs. [15–17] have shown that the packing effects upon β strongly depend upon the number, relative position, and orientation of the molecules in the clusters and therefore including all these aspects is a key step to determine accurate $\chi^{(2)}$. In this respect, simple schemes like the one presented in Ref. [17] turn out to be of practical interest.

The present work, which follows Ref. [17], adopts (1) the time-dependent Hartree–Fock (TDHF) scheme to account explicitly for the frequency dispersion of the first hyperpolarizability and (2) the configuration interaction (CI) method, limited to single excitations (CIS), to determine the lowest-energy excitation energies as well as to simulate the UV/visible electronic absorption spectra. In particular, this study focuses on the evolution of β as well as of the electronic absorption spectra as a function of the size and direction of growth of the MNA clusters. Moreover, the relationships between intra- and intermolecular charge transfer excitations and first hyperpolarizability are highlighted. Section 2 briefly summarizes the methodologies and computational aspects. Sections 3 and 4 present and discuss the results on the first hyperpolarizability and excitation energies, respectively, before the conclusions are drawn in Section 5.

2. Methodology and Computational Aspects

The geometric structures of the MNA molecule and the MNA crystals are taken from Ref. [5] and are similar to those used in Ref. [17]. As depicted in Figure 1, the MNA crystal is composed of (1, 4) stacked dimers.

The application of static and/or dynamic electrical fields to molecules and aggregates creates reorganization of the charge density that translates into induced multipole moments. Limiting the expansion to the second-order term in the electrical field, the ζ-component of the induced dipole moment at the frequency ω_σ reads

$$\Delta\mu_\zeta(\omega_\sigma) = \sum_\eta \alpha_{\zeta\eta}(-\omega_\sigma; \omega_1) E_\eta(\omega_1) + \frac{1}{2} K^{(2)} \sum_{\eta\xi} \beta_{\zeta\eta\xi}(-\omega_\sigma; \omega_1, \omega_2) E_\eta(\omega_1) E_\xi(\omega_2), \quad (1)$$

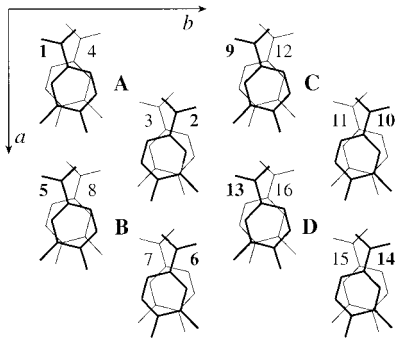

FIGURE 1. MNA crystal structure. *a*, *b*, and *c* refer to the crystallographic axes while A–D correspond to unit cell labels. The unit cell (A) contains four molecules (1–4).

where α is the polarizability, the ω_i are the pulsations of the incident beams, $\omega_\sigma = \sum_i \omega_i$, and the summations run over the field indices η and ξ associated with the Cartesian coordinates. $K^{(2)}$ is such that the β of different NLO processes converge toward the same static value. The static, second harmonic generation (SHG) and the electrooptic pockels effect (EOPE) responses are therefore given by $\beta(0; 0, 0)$, $\beta(-2\omega; \omega, \omega)$, and $\beta(-\omega; 0, \omega)$, respectively.

In addition to the summation-over-states (SOS) approach [19], the TDHF scheme [20] and its static analog, the coupled-perturbed Hartree–Fock (CPHF) [21] scheme, are certainly the most common procedures to evaluate the static and frequency-dependent electronic (hyper)polarizabilities. In this approach, a term representing the interaction between the external electric fields (which may contain both static and dynamic components) and the electric dipole operator is added to the Hamiltonian. Its effects upon the density matrix and the LCAO (linear combination of atomic orbitals) coefficients are obtained by expanding the TDHF/CPHF equation as a power series in the external electric fields and by solving it self-consistently order by order. The successive derivatives can then be used to evaluate the hyperpolarizabilities. In the present work the AM1 [22] version of the TDHF scheme [23] implemented in the MOPAC 2000 package [24] is used. It takes advantage of the $2n + 1$ theorem to express the first hyperpolarizability in terms of first derivatives of the LCAO coefficients. This approach is often called the "noniterative" approach although an iterative procedure is employed to get the first derivatives. When dealing with large MNA clusters, this approach appears to be an efficient means to combine accuracy and low

computational costs. Indeed, as shown in Ref. [17] as well as other investigations [4, 23], the AM1 Hamiltonian includes part of the electron correlation necessary to the description of nonlinear polarization effects in conjugated molecules because they provide first hyperpolarizability values that are smaller than the correlated MP2 results but larger than the CPHF ones. In addition, the ratios determining the importance of the crystal packing effects (for dimers) calculated at the MP2 level are reproduced to within 3% by the AM1 Hamiltonian [17]. In the evaluation of dynamic properties, the photon energy is set to 1.16 eV (1064 nm).

The excitation energies, ΔE_{ge}, of the MNA clusters have been determined using the CIS scheme based on Zerner's semiempirical INDO/S Hamiltonian [25–28], which uses the Nishimoto–Mataga–Weiss [25] expression for the two-center electron repulsion integrals. The CIS method based on semiempirical Hamiltonians has been shown to yield accurate predictions of transition energies because, on the one hand, most of the low-lying excitations are dominated by single excitations and, on the other hand, the parameters defining such Hamiltonians are fitted to spectroscopic data [28]. The CIS approach explicitly accounts for intra- and intermolecular charge transfer excitations—including their coupling—and, as demonstrated by Canuto et al. [29], it includes up to second order in perturbation theory the dispersion interactions between the subsystems of the supermolecule. In the case of a merocyanine dye forming head-to-tail aggregates, Millié et al. [30] have shown that the CIS scheme can be used to understand the relationship between the aggregate structure and collective optical properties. Our study differs however from ref. 30 by the almost parallel packing of the MNA molecules in the crystal, which can induce stable intermolecular charge transfers.

The CIS/INDO/S approach also provides the transition dipole moments between the ground and excited states, μ_{ge}, the excited state dipole moment, μ_{ee}, and the charge distributions of the excited states within the Mulliken population analysis. The oscillator strengths, $f_{ge} = 2/3\ \mu_{ge}^2 \Delta E_{ge}$, which are proportional to the transition probability and absorption intensity, are used to simulate the UV/visible electronic absorption spectra. Each transition is characterized by a full width at half maximum (FWHM) of 0.4 eV. The comparison between the ground- and excited-state charge distributions is used to characterize the nature of the transfer of charge accompanying the electronic excitation. The calculations have been performed using the MOS-F program [31]. A maximum of 100 (highest-energy) occupied and 100 (lowest-energy) unoccupied molecular orbitals ($N_{\mathrm{occ}} \times N_{\mathrm{unocc}} = 100 \times 100$) has been considered in the CIS expansions. Although such an approach deals with many excited states (up to 10,000), the truncation of the excitation manifold introduces size inconsistencies. This is in particular true if keeping the same single-excitation space while increasing the size of the clusters. To reduce most of this inconsistency, comparisons between clusters containing one, two, and three unit cells have been based on calculations using 30×30, 60×60, and 90×90 excited states, respectively. Figure 2 illustrates the effects of reducing the excitation manifold on the UV/visible absorption spectrum of the MNA unit cell. On the one hand, 30×30 excited states already reproduce the dominant feature of the low-energy electronic absorption spectrum of the MNA unit cell. On the other hand, contracting the excitation manifold to 10×10 leads to a global hypsochromatic shift and a decrease by almost a factor of 2 of the intensity of the second dominant peak located at 6–7 eV.

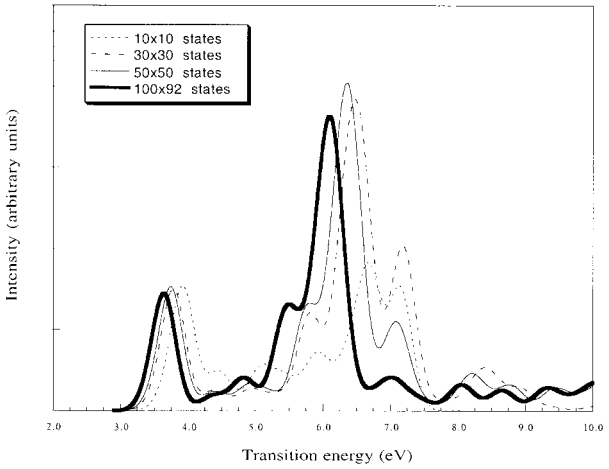

FIGURE 2. Simulated CIS/INDO/S electronic absorption spectrum of the MNA unit cell as a function of the size of the configuration space. The total number of occupied and unoccupied molecular orbitals is 116 and 92, respectively. FWHM = 0.4 eV.

3. Static and Dynamic First Hyperpolarizability

To address the packing effects upon β, increasingly large clusters of MNA have been built and their static, dc-Pockels, and SHG first hyperpolarizability tensors have been evaluated at the TDHF/

TABLE I

TDHF/AM1 static, dc-pockels, and SHG β_{aaa} (in au) and, in parentheses, crystal packing ratios for MNA clusters (1 au of $\beta = 3.206 \times 10^{-53}$ C^3 m^3 J^{-2} = 8.641×10^{-33} esu).

	Static	dc-Pockels	SHG
Monomer	1346	1599	2484
Dimer	1733	2026	3008
Unit cell (A)	3227 (0.931)	3760 (0.928)	5534 (0.920)
2 unit cells along *a* (A + B)	10,747 (1.550)	12,777 (1.577)	20,082 (1.669)
3 unit cells along *a*	23,124 (2.224)	28,099 (2.312)	46,985 (2.603)
2 unit cells along *b* (A + C)	5663 (0.817)	6546 (0.808)	9505 (0.790)
3 unit cells along *b*	7997 (0.769)	9259 (0.762)	13,376 (0.741)
2 unit cells along *c* (A + (A + *c*))	4568 (0.659)	5254 (0.648)	7541 (0.627)
3 unit cells along *c*	5872 (0.565)	6752 (0.555)	9591 (0.531)
4 unit cells (A + B + C + D)	17,243 (1.244)	20,303 (1.253)	30,310 (1.260)

See Eq. (2) for the definition of the packing ratio. A, B, (A + *c*), . . . are unit cells (Fig. 1). (A + *c*) refers to the unit cell obtained by translating unit cell A by one unit along the *c* axis.

AM1 level of approximation. Table I reports only the β_{aaa} diagonal tensor component because it dominates the second-order NLO response of all aggregates except the monomer. In the latter case, the nonnegligible value of the β_{baa}/β_{aaa} and β_{bbb}/β_{aaa} ratios (0.36 and −0.10, respectively, for SHG) results mostly from the inclination of the D/A axis of MNA with respect to the *a* crystallographic axis. Like in Ref. [17], the (1,4) stacked dimer of which the "C_2 axis" is parallel to the *a* crystallographic axis appears as the logical building block of MNA crystal because its β_{aaa} tensor component is more than one order of magnitude larger than all other components. The packing effect upon $\beta = \beta_{aaa}$ is therefore measured by the following ratio:

$$R^{\text{cluster}} = \frac{\beta^{\text{cluster}}}{N \times \beta^{(1,4)}}, \qquad (2)$$

where β^{cluster} and $\beta^{(1,4)}$ are the first hyperpolarizability of the cluster and of the isolated (1, 4) stacked dimer, respectively, and N the number of (1, 4) stacked dimers. The effective first hyperpolarizability of the (1, 4) stacked dimer within a given MNA cluster is defined by $\beta^{\text{eff}} = \beta^{(1,4)} \times R^{\text{cluster}}$. As in Ref. [17], the term "effective" includes both the modifications of the molecular wave functions and properties by the presence of surrounding molecules and the local field effects. The unit cell presents a packing ratio smaller than unity, which shows the reduction of the effective first hyperpolarizability of MNA when going from the dimer to the unit cell structure. The frequency dispersion and the type of second-order NLO phenomenon have a negligible (≤ 1%) influence on this reduction. For 1-D arrays of unit cells, the direction and amplitude of the packing effects depend upon the crystallographic axis along which the cluster grows. Indeed, for the *a* axis the packing ratio is larger than unity and strongly increases whereas it is smaller than unity and decreases for the *b* and *c* axes, the reduction being larger when stacking unit cells along the *c* axis. It is also noticeable that the packing-induced increase or decrease of the effective β is magnified in the case of dynamic processes as well as when the number and amplitude of the incident/generated optical frequencies become larger. The data on the A + B + C + D cluster (Fig. 1) demonstrate that for 2-D packing the effects tend to partially cancel each other.

This increase or reduction of the effective β is in qualitative agreement with simple electrostatics. Indeed, the presence of additional molecules along the field direction (corresponding to the situation where the cluster extends along the *a* axis) enhances the amplitude of the electric field at the reference site as a consequence of the induced dipole moments. Similarly, when enlarging the clusters in directions perpendicular to the electric field the fields created on the reference molecule by the induced dipole moments of the neighboring molecules counteract the external field and lead to smaller effective β values. In addition to these field-dependent (local field) effects, there also exist permanent field effects that originate from the mutual molecular interactions and account for the change of wave functions (and therefore properties) when going from the isolated to the in-crystal state. Such "dressing" effects are in particular important for polar molecules like D/A conjugated compounds,

TABLE II

CIS/INDO/S excitation energies (eV) of MNA clusters for the most significant intra- and intermolecular charge-transfer excited states.

	Intramolecular		Intermolecular	
Monomer	3.48	5.99		
Dimer	3.60	5.85, 6.14	2.60	
Unit cell (A)	3.65	5.60, 6.14, 6.20	2.05	3.89
2 unit cells along *a* (A + B)	3.50		1.92, 2.57	
3 unit cells along *a*	3.43		2.01	
4 unit cells along *a*	3.38		1.58	
2 unit cells along *b* (A + C)	3.87		2.11	3.44, 3.60, 3.85
3 unit cells along *b*	3.92		2.12	3.45, 3.60, 3.85
2 unit cells along *c* (A + (A + *c*))	3.93		2.12	3.63, 3.86
3 unit cells along *c*	3.99		2.12	3.59
4 unit cells (A + B + C + D)	3.75		1.43	

See Figure 1 and the caption of Table I for definition of the MNA clusters.

which have a large dipole moment. They explain why, for MNA, packing along the *a* axis increases the dipole moment per molecule (oriented parallel to the *a* axis) whereas the other directions of packing are characterized by a decrease of dipole moment. According to the strength of the D/A pair, these permanent field effects can reinforce or cancel the local field effects on the effective first hyperpolarizability. Indeed, the application of a static external electric field—which can reproduce the dominant dipolar intermolecular interactions—induces nonmonotonic variations of the molecular first hyperpolarizability [32]. The MNA molecule corresponding to the region where the first hyperpolarizability increases with the dipole moment; the two effects strengthen. In Section 4, we show how these variations in the effective first hyperpolarizability are related to the characteristics of the excited states.

4. Electronic Absorption Spectra

Table II lists the excitation energies of MNA clusters for the most significant excited states. Figures 3–7 provide the corresponding simulated electronic absorption spectra, which have been grouped to highlight the size and directionality effects. In the monomer, the typical intramolecular charge transfer excited state [3] corresponds to an excitation energy of 3.48 eV and a transfer of 0.6 *e* (*e* is the magnitude of the electron charge) from the amino group and the phenyl ring to the nitro moiety. It is also associated with a large change in dipole moment ($\Delta\mu_{ge} = \mu_{ee} - \mu_{gg}$). As shown in Figure 3, it dominates the low-energy absorption spectrum whereas the broad absorption band around $\Delta E = 6.0$ eV is due to excited states having small or opposite transfers of charge. By referring to the SOS expression of β and limiting it to the dipolar-type terms, $\beta = 6\Delta\mu_{ge}\mu_{ge}^2/\Delta_{ge}^2$, it is straightforward to understand that the low-energy intramolecular charge transfer excited states contribute significantly to β.

In the dimer, due to intermolecular interactions, the low-energy intramolecular charge transfer excited state splits into two charge transfer excited states. The lower state ($\Delta E = 3.40$ eV) is characterized by a small dipole moment transition while the upper state ($\Delta E = 3.60$ eV) presents a strong ab-

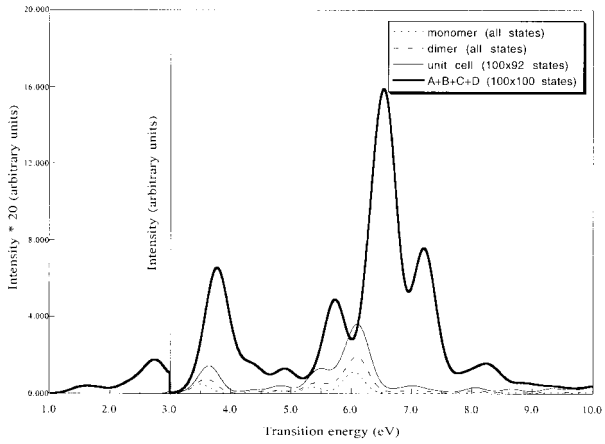

FIGURE 3. Simulated CIS/INDO/S electronic absorption spectrum of the monomer, dimer, unit cell, and four unit cell cluster (A + B + C + D). FWHM = 0.4 eV.

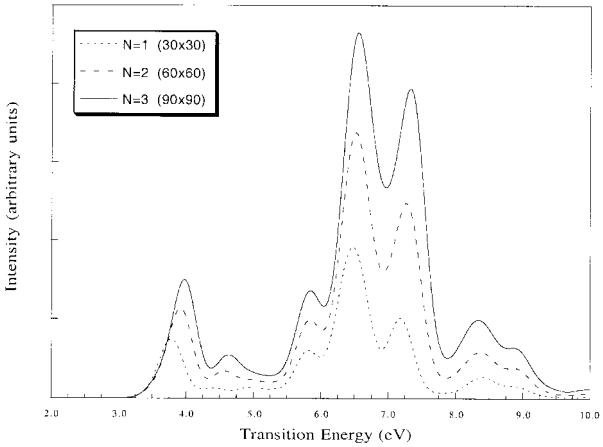

FIGURE 4. Simulated CIS/INDO/S electronic absorption spectrum of increasingly large arrays of MNA unit cells extending along the *c* crystallographic axis. FWHM = 0.4 eV. N is the number of unit cells.

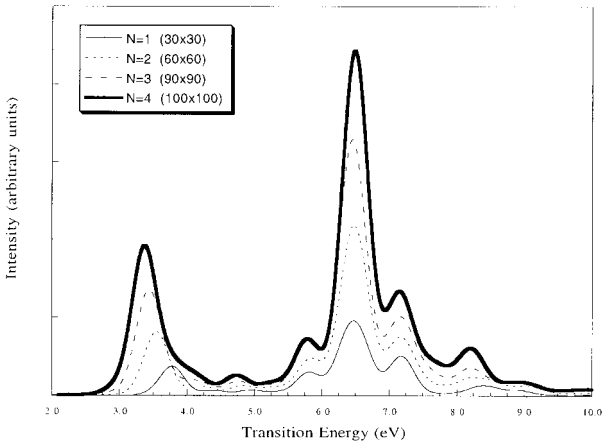

FIGURE 6. Simulated CIS/INDO/S electronic absorption spectrum of increasingly large arrays of MNA unit cells extending along the *a* crystallographic axis. FWHM = 0.4 eV. N is the number of unit cells.

sorption. In fact, a detailed analysis of the CIS coefficients shows that the excited wave functions of the dimer are developed over excitations involving MOs delocalized on the two monomers, and thus these two states contain both intra- and intermolecular contributions. However, the ground- vs. excited-state Mulliken charge distributions show that the amount of intermolecular charge transfer is small for these two transitions (ΔE = 3.40 eV, 3.60 eV). A similar analysis can be made for the excitations that dominate the absorption spectrum in the 5- to 7-eV region. On the other hand, the excited state corresponding to ΔE = 2.60 eV is associated with a transfer of 0.26 *e* between the two molecules whereas for higher-energy excitations ($\Delta E \geq 6.0$ eV) the intermolecular charge transfers can attain 0.6–0.9 *e*. However, these states are associated with small μ_{ge} and are therefore not visible in Figure 3. Subsequently their contributions to β are expected to be negligible.

In the unit cell there are additional interactions that lead to four low-energy intramolecular charge transfer excitations (ΔE = 3.41, 3.45, 3.59, and 3.65 eV). Among them, the higher-energy state presents again the largest μ_{ge} value and is mostly responsible for the first absorption band (Figs. 2 and 3). The transitions at 5.60, 6.14, and 6.20 eV are also characterized by large transition dipole moments and result in intense absorptions (Figs. 2 and 3). Like in

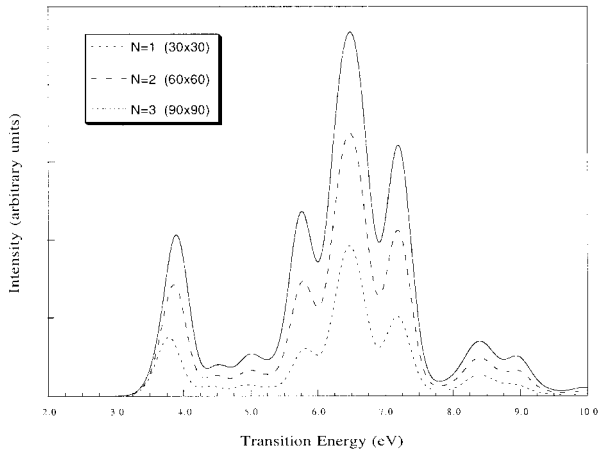

FIGURE 5. Simulated CIS/INDO/S electronic absorption spectrum of increasingly large arrays of MNA unit cells extending along the *b* crystallographic axis. FWHM = 0.4 eV. N is the number of unit cells.

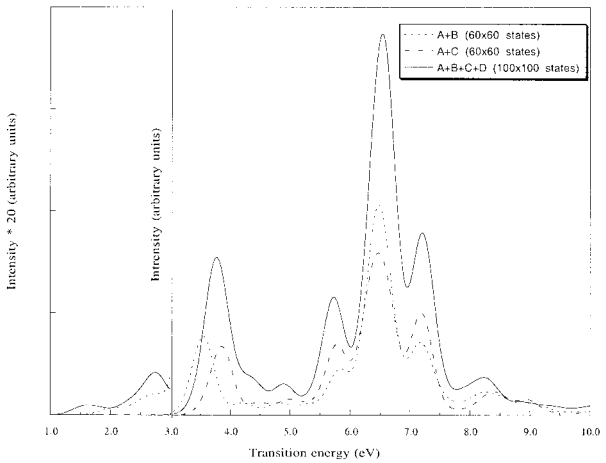

FIGURE 7. Simulated CIS/INDO/S electronic absorption spectrum of the (A + B), (A + C), and (A + B + C + D) clusters. FWHM = 0.4 eV.

TABLE III

CIS/INDO/S characteristics of the dominant low-energy intramolecular charge transfer excited state for different 1-D arrays of MNA.

	ΔE_{ge} (eV)	μ_{ge} (D)	$\Delta\mu_{ge}$ (D)	f_{ge}	RI
Unit cell (A)	3.65	3.74	9.33	0.194	1.00
2 unit cells along *a* (A + B)	3.50	5.54	10.29	0.407	1.05
2 unit cells along *b* (A + C)	3.87	4.98	10.32	0.364	0.94
2 unit cells along *c* (A + (A + *c*))	3.93	4.50	10.08	0.302	0.78

Relative intensity (RI) = $f^{\text{cluster}}/(N \times f^{\text{unit cell}})$, with N the number of unit cells in the cluster and f the corresponding oscillator strength.

the dimer, the first excited state (ΔE = 2.05 eV) presents a substantial character of intermolecular charge transfer and is associated with a negligible μ_{ge}. At ΔE = 3.89 eV and at higher excitation energies, there are other transitions having important intermolecular charge transfer character and small oscillator strength. The ΔE = 3.89 eV transition corresponds to the transfer of almost one electron from the (1, 4) to the (2, 3) stacked dimer (see Fig. 1). It is characterized by a dipole moment variation almost antiparallel to the unit cell dipole moment. This antiparallel configuration accounts for its stabilization.

We now turn to the study of the evolution of the electronic absorption spectra as a function of number of unit cells in 1-D arrays. When stacking unit cells along the *c* axis, the first absorption band ($\Delta E \sim 4$ eV) presents a hypsochromatic shift (Fig. 4). This band contains several intramolecular charge transfer transitions, the most intense of which has the highest ΔE value. Moreover, its relative intensity decreases with respect to the single unit cell case (Table III). On the other hand, for the triple band at higher energy there is no shift and the intensity grows almost linearly with the number of unit cells. The first transition (ΔE = 2.12 eV) keeps an important intermolecular charge transfer component and a weak transition dipole moment. The excited states associated with the transfer of electron from the (1, 4) to (2, 3) stacked dimers (as well as their analogs in the other unit cells) remain around 3.6–3.9 eV while the corresponding μ_{ge} becomes larger than in the case of a single unit cell. These intermolecular charge transfer transitions remain, however, much weaker than the intramolecular charge transfer transitions that dominate the spectra in the 4-eV region.

The packing along the *b* crystallographic axis induces a little shift in the positions and a small decrease in the relative intensities of the absorption peaks (Fig. 5). In addition to the excitation-induced electron transfer from the (1, 4) to (2, 3) stacked dimers belonging to the same unit cell (ΔE = 3.85 eV for two unit cells along *b*), there also exist transfers between dimers belonging to adjacent unit cells. In particular, at ΔE = 3.44 eV the excited state corresponds to a transfer of almost one *e* from the (2, 3) to (9, 12) stacked dimers (see Fig. 1). Again, their transition dipole moments are small and most of the first hyperpolarizability can be traced back to the intramolecular charge transfer excitations.

The situation is different when stacking unit cells along the *a* crystallographic axis because it is associated with a bathochromatic shift of the first absorption band, which remains "intramolecular" as well as because the relative intensity increases with the number of unit cells. In these aggregates, intermolecular charge transfers take place over much longer distances. In the two, three, and four unit cell aggregates, the lower-energy excited states of this type are characterized by $\Delta\mu_{ge}$ as large as 46, 86, and 126 Debye corresponding to ΔE of 2.57, 2.01, and 1.58 eV, respectively. Although their transition dipole moments are still small, they will play a role in the NLO responses when approaching resonance. In addition to these states, there are a number of intermolecular charge transfer excited states below the dominant intramolecular band that present nonnegligible oscillator strengths and energies in the 2.0- to 2.5-eV region and, therefore, contribute slightly to β.

Finally, when considering a 2-D building (A + B + C + D) the first dominant peak (ΔE = 3.75 eV) is, as expected, slightly at higher energy than in the (A + B) cluster (ΔE = 3.50 eV) but at lower energy than the (A + C) cluster (ΔE = 3.87 eV) (Fig. 7). Nevertheless, the most important point is the appearance of a small peak at ΔE = 1.43 eV that corresponds to a stabilized intermolecular charge transfer state presenting a *less* negligible transition dipole moment.

5. Further Discussions, Conclusions, and Outlook

The static and dynamic first hyperpolarizability of MNA clusters has been evaluated at the TDHF/AM1 level to determine the crystal packing effects upon the NLO responses. When building 1-D arrays of MNA unit cells along the *a* crystallographic axis, the effective hyperpolarizability or the crystal packing ratio strongly increases whereas stacking unit cells along the *b* and *c* axes leads to a reduction of these quantities. These effects are magnified in the case of frequency-dependent phenomena. These "direction" differences have been explained, on qualitative grounds, in terms of both the differences between the applied and local electric fields and of the permanent electric field effects.

To further rationalize these effects, the excitation energies of the MNA clusters have been determined at the CIS/INDO/S level of approximation and the corresponding UV/visible absorption spectra have been simulated. For all clusters, the spectra display an intense low-energy absorption band in the 3.0- to 4.0-eV region. The corresponding transitions present the strong intramolecular charge transfer character, which is known to give rise to important β contributions [3]. Indeed, these excited states are associated with large transition dipole moments, μ_{ge}, and large variations of the dipole moment upon excitation, $\Delta\mu$. When stacking unit cells along the *b* and *c* crystallographic axes, this absorption band exhibits a hypsochromatic shift whereas for the third crystal direction the shift is bathochromatic. Moreover, the transition dipole moment (Table III) is larger for the stacking along the *a* axis than for stacking along its perpendicular directions whereas the variations of $\Delta\mu$ are smaller. These behaviors can help in rationalizing the differences in the evolution of the effective β value when building 1-D arrays along the *a*, *b*, or *c* crystallographic axes.

In addition to these intramolecular charge transfer excited states, which dominate the UV/visible absorption spectra, a number of intermolecular charge transfer states have been detected. In the small MNA aggregates as well as for clusters extending along the *b* and *c* crystallographic axes, these excited states possess small transition dipole moments although the corresponding energies of excitation can be as small as 2 eV. On the other hand, when stacking MNA unit cells along the *a* axis (or simultaneously along the *a* and *b* axes) these intermolecular charge transfer states acquire nonnegligible transition dipole moments and their excitation energies go from 2.6 to 1.4 eV. As a consequence, it can be understood (1) that, although small, their contributions to β increase, especially for dynamic processes, and (2) that in the near resonant region they will lead to convergence problems of the TDHF scheme, which lacks damping effects. Such intermolecular charge transfer excited states are stabilized by electrostatic interactions because the change in dipole moment is almost antiparallel to the dipole moment of the cluster.

It is important to point out that the comparison between the first hyperpolarizability and excited-state characteristics should be kept on qualitative grounds because, due to program availability, the former have been evaluated at the TDHF/AM1 level whereas the second have been calculated with the CIS/INDO/S approach.

In these polar systems, where excited states exhibiting multiple charge transfers can be stabilized by electrostatic interactions with the surroundings, it appears of interest to consider the effects of including double, triple, ... excitations on the optical and electronic properties of MNA clusters. However, due to enormous computational requirements, these calculations become rapidly prohibitive and alternative solutions like the one proposed in Ref. [33] have to be considered to characterize the collective electronic and optical behavior of MNA crystals.

ACKNOWLEDGMENTS

M.G. thanks the "Fonds pour la Formation et la Recherche dans l'Industrie et dans l'Agriculture" (FRIA) for financial support as well as the European community for his doctoral Marie Curie Fellowship. E.B. thanks the Fonds Spécial de Recherches of the Facultés Universitaires Notre-Dame de la Paix for her postdoctoral grant. B.C. thanks the Belgian National Fund for Scientific Research for his Senior Research Associate position. The authors thank Profs. D. Liotard and A. Fritsch for fruitful discussions and Prof. B. Kirtman for careful reading of the article. The calculations have been performed thanks to computing time made available by the SiMoA (Simulation et Modélisation en Aquitaine, France) as well as on the Pentium III cluster of the CTA lab, for which the authors acknowledge the financial support of the FNRS.

References

1. Nalwa, H. S., Ed. Handbook of Advanced Electronic and Photonic Materials and Devices, Vol. 9, Nonlinear Optical Materials; Academic Press: New York, 2001.

2. Bosshard, C.; Sutter, K.; Prêtre, P.; Hulliger, J.; Flörsheimer, M.; Kaatz, P.; Günter, P. Organic Nonlinear Optical Materials, In: Kajzar, F., Ed. Advances in Nonlinear Optics; Gordon and Breach Publishers: Basel, 1995.
3. Kanis, D. R.; Ratner, M. A.; Marks, T. J. Chem Rev 1994, 94, 195.
4. Champagne, B.; Kirtman, B. In: Nalwa, H. S., Ed. Handbook of Advanced Electronic and Photonic Materials and Devices, 2001; Chapter 2, p 63.
5. Lipscomb, G. F.; Garito, A. F.; Narang, R. S. J Chem Phys 1981, 75, 1509.
6. Champagne, B.; Bishop, D. M. Adv Chem Phys (in Press).
7. Chemla, D. S.; Oudar, J. L.; Jerphagnon, J. Phys Rev B 1975, 12, 4534.
8. Dykstra, C. E. J Comput Chem 1988, 9, 476.
9. Kirtman, B.; Dykstra, C. E.; Champagne, B. Chem Phys Lett 1999, 305, 132.
10. Munn, R. W. Mol Phys 1996, 89, 555.
11. Munn, R. W. J Mol Electron 1986, 2, 35; Munn, R. W. Mol Phys 1988, 64, 1.
12. See, e.g., Munn, R. W. Int J Quantum Chem 1992, 43, 159; Munn, R. W.; Shuai, Z.; Brédas, J. L. J Chem Phys 1998, 108, 5975; Reis, H.; Papadopoulos, M. G.; Munn, R. W. J Chem Phys 1998, 109, 6828.
13. Reis, H.; Papadopoulos, M. G.; Hättig, C.; Ángyán, J. G.; Munn, R. W. J Chem Phys 2000, 112, 6161.
14. Zyss, J.; Berthier, J. G. J Chem Phys 1982, 77, 3635.
15. Yasukawa, T.; Kimura, T.; Uda, M. Chem Phys Lett 1990, 169, 259; Di Bella, S.; Ratner, M. A.; Marks, T. J. J Am Chem Soc 1992, 114, 5849.
16. Hamada, T. J Phys Chem 1996, 100, 8777.
17. Castet, F.; Champagne, B. J Phys Chem A 2001, 105, 1366.
18. Kurtz, H. A.; Stewart, J. J. P.; Dieter, K. M. J Comput Chem 1990, 11, 82.
19. Orr, B. J.; Ward, J. F. Mol Phys 1971, 20, 513.
20. Sekino, H.; Bartlett, R. J. J Chem Phys 1986, 85, 976; Karna, S. P.; Dupuis, M. J Comput Chem 1991, 12, 487.
21. Langhoff, P. W.; Karplus, M.; Hurst, R. P. J Chem Phys 1966, 44, 505.
22. Dewar, M. J. S.; Zoebisch, E. G.; Healy, E. F.; Stewart, J. J. P. J Am Chem Soc 1985, 107, 3902.
23. Korambath, P.; Kurtz, H. A. In: Karna, S. P.; Yeates, A. T. Eds. Nonlinear Optical Materials, Theory and Modeling, (ACS Symposium Series 628; ACS: Washington, DC, 1996; p 133.
24. MOPAC2000. Fujitsu, 1999.
25. Ridley, J. E.; Zerner, M. C. Theor Chim Acta Berl 1973, 32, 111.
26. Ridley, J. E.; Zerner, M. C. Theor Chim Acta Berl 1976, 42, 223; Bacon, A. D.; Zerner, M. C. Theor Chim Acta Berl 1979, 53, 21.
27. Zerner, M. C.; Loew, G. H.; Kirchner, R. F.; Mueller-Westerhoff, U. T. J Am Chem Soc 1980, 102, 589.
28. Zerner, M. C. In: Lipkowitz, K. B.; Boyd, D. B., Eds., Reviews of Computational Chemistry, Vol. 1; VCH: New York, 1991; p 313; Martin, C. H.; Zerner, M. C. In: Solomon, E. I.; Lever, A. B. P., Eds. Inorganic Electronic Structure and Spectroscopy, Vol. 1; Wiley: New York, 1999; p 555.
29. Canuto, S.; Coutinho, K.; Zerner, M. C. J Chem Phys 2000, 112, 7293.
30. Millié, P.; Momicchioli, F.; Vanossi, D. J Phys Chem B 2000, 104, 9621.
31. MOS-F (semiempirical Molecular Orbital package for Spectroscopy, Fujitsu), V4, 1999.
32. Kirtman, B.; Champagne, B.; Bishop, D. M. J Am Chem Soc 2000, 122, 8007.
33. Brunaud, G.; Castet, F.; Fritsch, A.; Kreissler, M.; Ducasse, L. J Phys Chem B 2001, 105, 12665.